JOURNAL OF GEOPHYSICAL RESEARCH, VOL. 111, A09303, doi:10.1029/2006JA011736, 2006

Vibrational relaxation of $CO_2(\nu_2)$ by atomic oxygen

Karen J. Castle,[1] Katherine M. Kleissas,[1] Justin M. Rhinehart,[1]
Eunsook S. Hwang,[2] and James A. Dodd[3]

Received 22 March 2006; revised 3 May 2006; accepted 9 May 2006; published 13 September 2006.

[1] In the Earth's upper atmosphere, collisions with ambient O atoms efficiently excite the CO_2 [00^00] vibrational ground-state population to the first excited, [01^10] or ν_2, vibrational bend state. Subsequent relaxation of the ν_2 population occurs through spontaneous emission of 15-μm radiation. Much of this radiation escapes into space, thereby removing ambient kinetic energy from the atmosphere. This cooling mechanism is especially important at altitudes between the mesopause and the lower thermosphere, approximately 80–120 km, where the O-atom density is relatively high and the kinetic temperature is rising. Laboratory measurements have been performed to better characterize the $CO_2(\nu_2)$-O vibrational relaxation rate coefficient $k_O(\nu_2)$. A 266-nm laser pulse photolyzed trace amounts of O_3 in a CO_2-O_3-rare gas mixture, simultaneously creating O atoms and raising the gas temperature to create a nonequilibrium CO_2 vibrational distribution. Transient diode laser absorption spectroscopy was used to monitor CO_2 vibrational level population reequilibration. A global nonlinear least squares fitting technique was used to interpret the kinetic data, yielding $k_O(\nu_2) = (1.8 \pm 0.3) \times 10^{-12}$ cm^{3}s^{-1}. The result is in good agreement with previous laboratory measurements, with published $k_O(\nu_2)$ values in the $(1.2–1.5) \times 10^{-12}$ cm^{3}s^{-1} range and at the low end of the $(2–6) \times 10^{-12}$ cm^{3}s^{-1} range estimated from the analysis of upper atmospheric data.

Citation: Castle, K. J., K. M. Kleissas, J. M. Rhinehart, E. S. Hwang, and J. A. Dodd (2006), Vibrational relaxation of $CO_2(\nu_2)$ by atomic oxygen, *J. Geophys. Res.*, *111*, A09303, doi:10.1029/2006JA011736.

1. Introduction

[2] The upper atmospheres of Earth, Venus, and Mars all cool by radiative emission from vibrationally excited CO_2, particularly from the [01^10] bending mode at 15 μm. In the terrestrial upper mesosphere–lower thermosphere (UMLT), roughly 80–110 km, emission by CO_2 is essentially the only mechanism by which cooling occurs. At these altitudes, the relatively low gas collision frequency, about 1000 s^{-1} at 100 km, results in incomplete collisional coupling between the populations of the various CO_2 vibrational levels. Because of this phenomenon, the vibrational populations of CO_2 depart from local thermodynamic equilibrium (LTE) [*Lopez-Puertas et al.*, 1998; *Wintersteiner et al.*, 1992]. The vibrational temperatures, which can differ dramatically from the local kinetic temperature, must be accurately determined in order to calculate the cooling rate. In turn, computing the vibrational temperatures requires knowledge of each mechanism by which CO_2 vibration-rotation populations exchange energy with their surroundings.

[3] Atomic oxygen plays an important role by enhancing CO_2 cooling ability in the Earth's UMLT region [*Houghton*, 1970]. Conversion of ambient kinetic energy to CO_2 internal energy is governed by collisions with O despite its small mixing ratio at 100 km, that is, a few parts per hundred relative to the major atmospheric species, N_2 and O_2. The collisional process effectively raises the vibrational temperature of the CO_2, thereby increasing the population in the ν_2 modes and the amount of spontaneous emission and cooling via 15-μm emission. Here the focus is on the lowest bend-excited state, CO_2 [01^10], which is particularly important since it is directly coupled to the large ground-state population. The collisional excitation process is given by:

$$O + CO_2(00^00) \xrightarrow{k_1} O + CO_2(01^10), \quad (1)$$

where k_1 is the rate coefficient for vibrational up-pumping. The energy resident in the CO_2 vibration may then be converted back to translational energy by subsequent collisions, or the molecule may radiate by spontaneous or stimulated emission. If the radiated energy escapes a local volume of the atmosphere, a cooling of that volume is achieved.

[4] The reverse process of equation (1) is typically studied in the laboratory. That is, the rate coefficient associated with vibrational deactivation through collisions with atomic oxygen is measured:

$$O + CO_2(01^10) \xrightarrow{k_{-1}} O + CO_2(00^00). \quad (2)$$

The rate coefficients k_1 and k_{-1} are related through the principle of detailed balance by the equilibrium constant K,

[1]Department of Chemistry, Bucknell University, Lewisburg, Pennsylvania, USA.
[2]Stewart Radiance Laboratory, Bedford, Massachusetts, USA.
[3]Space Vehicles Directorate, Air Force Research Laboratory, Hanscom Air Force Base, Massachusetts, USA.

0148-0227/06/2006JA011736$09.00

which defines the CO_2 [01^10]/CO_2 [00^00] population ratio as:

$$\frac{k_1}{k_{-1}} \equiv K = 2e^{\frac{-667}{kT}} = 0.078 \qquad (\text{at } 296\,\text{K}). \tag{3}$$

Note that in the discussion below, the rate coefficient for relaxation of CO_2 [01^10] by O is denoted $k_O(\nu_2)$ in place of k_{-1}.

[5] Several laboratory measurements of $CO_2(\nu_2)$-O vibrational relaxation have been performed, with published $k_O(\nu_2)$ values spanning the $1.2-1.5 \times 10^{-12}$ cm^3s^{-1} range [*Khvorostovskaya et al.*, 2002; *Pollock et al.*, 1993; *Shved et al.*, 1991]. For M = N_2 and O_2, the corresponding $k_M(\nu_2)$ values are in the mid-10^{-15} cm^3s^{-1} range, about 3 orders of magnitude smaller than $k_O(\nu_2)$ [*Lunt et al.*, 1985; *Siddles et al.*, 1994]. Thus the studies have confirmed that the UMLT minor constituent O, with a mixing fraction of a few parts per hundred at 100 km, governs the collisional excitation of the CO_2 [01^10] level. However, a number of analyses of 15-μm UMLT emissions have suggested an even larger value of $k_O(\nu_2)$, with one landmark publication deriving the value $k_O(\nu_2) = (6 \pm 3) \times 10^{-12}$ cm^3s^{-1} [*Sharma and Wintersteiner*, 1990]. In light of the uncertainty in $k_O(\nu_2)$, it was felt that a laboratory study in which all low-lying CO_2 vibrational populations could be directly monitored would be of value. The approach described below incorporating relaxation kinetics with time-resolved IR absorption detection of CO_2 provides this capability.

2. Experimental

2.1. Basic Technique

[6] The temperature-jump technique has been used for this work because of its ease of implementation and its well-defined kinetics. A temperature perturbation is applied to the system that temporarily disturbs the equilibrium condition. The relevant species concentrations are then monitored as a function of time as they return to equilibrium [*Bernasconi*, 1976]. For a two-level collisionally coupled system, the kinetic equations defining the return to equilibrium can be linearized regardless of the size of the perturbation. In the present work, assuming an adequate O-atom density, the CO_2[00^00] and [01^10] vibrational levels are coupled solely through collisions with O. For the simple two-level system described in equation (2) the rate coefficient governing the return to equilibrium, k_{r1}, is given by

$$k_{r1} = k_1 + k_{-1}. \tag{4}$$

Combined with equation (3), the relationship between $k_O(\nu_2)$ and k_{r1} is given by

$$k_O(\nu_2) = 0.928 k_{r1}. \tag{5}$$

Following the perturbation the population increases (or decreases, depending on whether the monitored population is initially underpopulated or overpopulated) with single-exponential time dependence. The characteristic decay rate plotted as a function of O-atom concentration allows the determination of k_{r1}, from which $k_O(\nu_2)$ is derived using equation (5).

2.2. Apparatus Details

[7] Several changes have been made in this work compared with the preliminary apparatus design described in a previous manuscript [*Castle et al.*, 2003]. A block diagram of the experimental setup is given in Figure 1. Most significantly, the reaction cell length has been increased by nearly an order of magnitude to 96.0 cm, allowing the use of very small CO_2 mole fractions without sacrificing the ability to detect the transient absorption signal. The reaction cell inside diameter (ID) is 25.4 mm. Gases were slowly flowed through the cell during the experiment. Mass flow rates, controlled using MKS MassFlo flow controllers, were typically 0.2 standard atm cm^{-3} min^{-1} (sccm) CO_2, 6 sccm Ar, 50 sccm Xe, and small, variable amounts of O_3. To encourage a homogeneous gas mix in the laser pump/probe region, the CaF_2 cell windows were inset on 12.7-mm diameter, 3-cm-long Pyrex stalks, and gases were introduced and removed through four 0.48-cm ID Teflon tubes spaced equally around the outer portion of the cell end. With the exception of O_3, partial pressures were taken to be proportional to the individual mass flow rates. A throttled roughing pump maintained a total gas pressure of 5–12 torr, measured with an MKS Baratron capacitance manometer teed off the reaction cell. This pressure range served to minimize CO_2 [01^10] and O-atom loss from the reaction volume through diffusion effects. Ozone was generated by passing O_2 through an Ozomax ozonator and was stored on a silica gel column cooled to −65°C. After pumping off the residual O_2, Ar was flowed through the column to carry O_3 into the reaction cell.

[8] The current setup allowed for direct measurement of O_3 concentrations in the reaction cell along the longitudinal axis. A UV monochromator (Optometrics) and photomultiplier tube were used to detect 120-Hz sinusoidal, 254-nm Hg lamp output. Given the O_3 absorption cross section $\sigma_{254} = 1.15 \times 10^{-17}$ cm^2, the ratio of the transmitted light intensity with and without O_3 present allowed the determination of the O_3 partial pressure. This pressure was maintained in the 1–100 mTorr range by adjusting the temperature of the column and/or the flow rate of the Ar carrier gas with a needle valve. The absorption measurements were performed just before and after data collection whenever the O_3 flow was adjusted.

2.3. Species Excitation and Detection

[9] The time-evolving population of the [01^10] vibrational level of CO_2 was monitored using tunable diode laser absorption spectroscopy (TDLAS) on the $\Delta\nu_3 = 1$ asymmetric stretch transition. The ν_3 absorption bands of CO_2 are very intense, providing a sensitive detection method. The frequency of the diode laser (Laser Components) was fixed at the peak of a CO_2 [01^10] absorption line, and the transient absorption signal was monitored using an Infrared Associates liquid-nitrogen cooled InSb detector. A 3.0–5.0 μm antireflection-coated Ge window and a 3.8–4.8 μm band-pass filter (Janos Technology) were employed to reduce the amount of scattered light reaching the InSb detector. Rotational state populations are typically equilibrated on a timescale that is short compared with vibrational

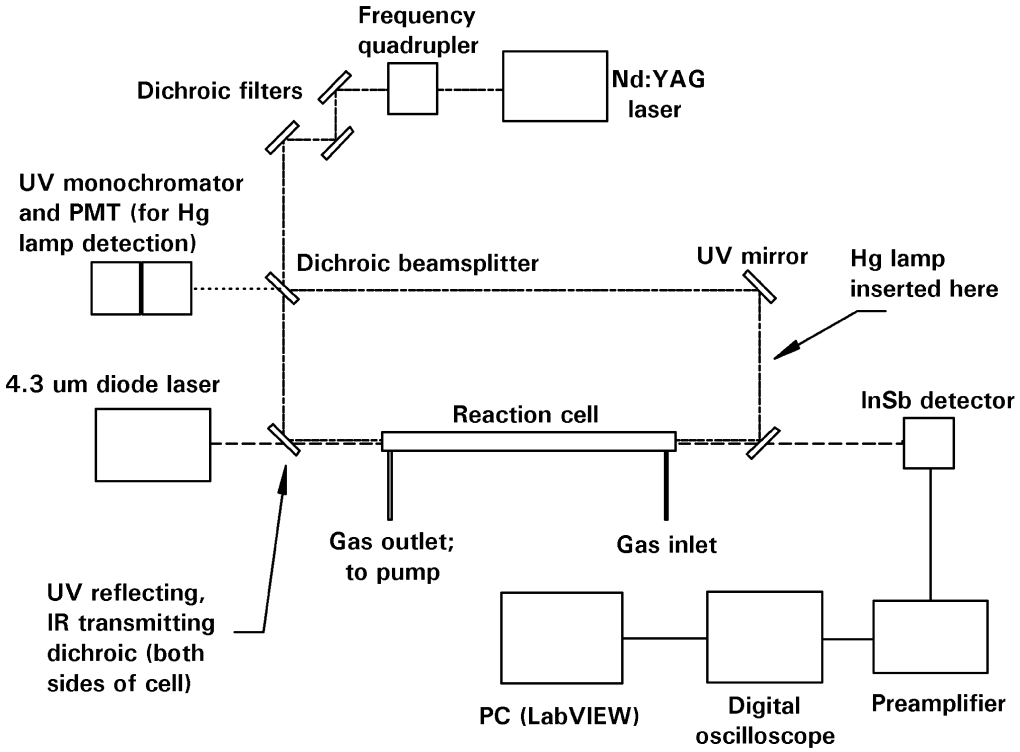

Figure 1. Overview of experimental apparatus for the $CO_2(\nu_2)$-O energy transfer studies. The 266-nm photolysis beam is shown as the short-dashed line, and the 4.3-μm probe beam is shown as the long-dashed line. The pump and probe beams are offset for clarity. The irises, lenses, optical filters, and chopper associated with the diode laser beam are not shown. Periodically, the two beams were blocked, and the Hg lamp was inserted to measure the O_3 concentration in the reaction cell. The 254-nm lamp emission was detected by the UV monochromator (PMT detector shown at left). The transient IR signal from the InSb detector was passed through a preamplifier to a digital oscilloscope and then to a PC for storage and analysis. See text for further discussion.

populations; thus any one of several rotational level populations could be used to extract the desired kinetic information. Figure 2 shows an energy level diagram for CO_2 vibrational levels up to 3000 cm^{-1}, and Figure 3 shows a representative CO_2 absorption spectrum. The signal has been ratioed by the background, taking into account the diode laser fluence, and allowing more convenient comparison of absorption strengths. The assignments shown were made with the help of the HITRAN database [*Rothman et al.*, 2005]. The experiment was aided by introducing several torr of inert bath gas to pressure-broaden the absorption, similar to others' strategy (L. F. Phillips, personal communication, 2001).

[10] Pressure-broadening allowed the diode laser frequency to drift slightly during the course of data taking, without leading to an unwanted variation in the absorption signal. The CO_2 (01^10)-$[01^11]$ $P(33)$ transition at 2307.653 cm^{-1} was used to obtain the value of $k_O(\nu_2)$.

[11] The O_3 was photolyzed using 266-nm frequency-quadrupled Continuum Surelite Nd:YAG laser pulses of approximately 17-mJ energy (see below), the photolysis laser running at 5.4 Hz. The photolysis simultaneously produced O atoms and induced a temperature jump of the gas mixture, promoting vibrational excitation of the CO_2. Dichroic beam combiners on CaF_2 substrates were used to overlap the photolysis and detection laser beams in a collinear geometry,

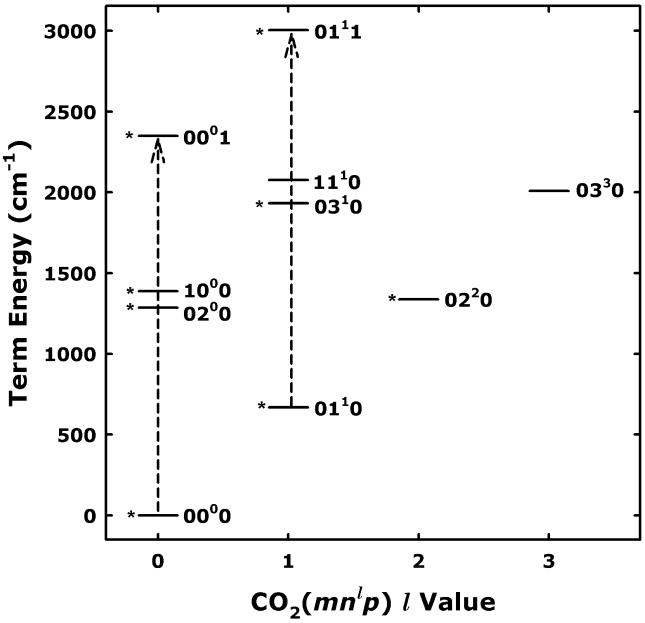

Figure 2. Nine lowest-energy CO_2 vibrational levels, plus the (01^11) level, plotted as a function of vibrational angular momentum l. Two $\nu_3 \rightarrow \nu_3 + 1$ diode laser absorption transitions are indicated. Populations labeled with the asterisk have been detected in this study.

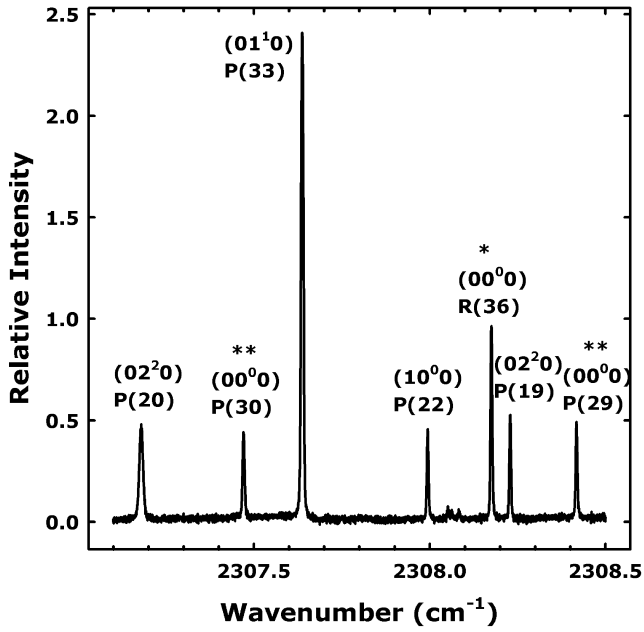

Figure 3. CO_2 absorption spectrum exciting $\nu_3 \rightarrow \nu_3 + 1$ bands, obtained using diode laser absorption spectroscopy with a static gas cell. The vibration-rotation designations of the various lower states are noted. The single asterisk refers to the $^{16}O^{13}C^{16}O$ isotope, and the double asterisk refers to the $^{16}O^{12}C^{18}O$ isotope.

as shown in Figure 1. Two irises were inserted in the diode laser path to restrict the diameter of the detection beam to 1.5 mm, smaller than the 5.7-mm diameter photolysis beam (see below). The photolysis pulses triggered data acquisition by a PC-interfaced Tektronix TDS3014B oscilloscope, and the population time evolution was extracted from the resulting transient absorption.

[12] One disadvantage of the long optical path length is the likelihood of a photolysis laser fluence axial gradient due to O_3 absorption. The photolysis laser pulse is slightly absorbed, especially at the higher O_3 densities. For 90% of the data, however, the nominal absorbance $A < 0.2$ over the 96-cm path length, with $A < 0.05$ for most of the data. For the 17-mJ laser fluence the effective absorbance is lower owing to partial bleaching. To minimize any residual axial fluence gradient the photolysis laser pulses were divided using a 50:50 beam splitter and directed through both ends of the reaction cell. The O_3 was dissociated by the photolysis laser to yield $O(^1D) + O_2(^1\Delta_g)$ (85% branching fraction) and $O(^3P) + O_2(^3\Sigma_g^-)$ (15%). Nascent $O(^1D)$ atoms were efficiently quenched to $O(^3P)$ by the predominantly Xe bath gas, with quenching rate coefficient $k_Q(Xe) = 7.5 \times 10^{-11}$ cm^{3}s^{-1} [*Schofield*, 1978]. With >0.4 torr Xe, the $O(^1D)$ lifetime is less than 1 μs. CO_2 is also an efficient quencher, with $k_Q(CO_2) = 1.1 \times 10^{-10}$ cm^{3}s^{-1} [*Sander et al.*, 2002], and its mole fraction (typically 0.0035) was minimized in order to discourage formation of high υ level populations that could cascade downward through the ν_2 level and bias the relaxation measurement. In one trial, the CO_2 mixing fraction was lowered to 0.0015, with no discernable difference in the results. Residual O_3 will also react with $O(^1D)$ to form a mix of O_2 and O products, with $k_Q(O_3) = 2.4 \times 10^{-10}$ cm^{3}s^{-1} [*Sander et al.*, 2002], but this will be a minor process owing to its small mixing ratio of ≤2% relative to Xe.

[13] Simulations have shown that O atoms are long-lived, limited only by three-body recombination and transport loss out of the reaction volume, which are expected to have timescales 10–1000 times longer than CO_2 [01^{1}0] relaxation. $O(^3P)$ reacts very slowly with residual O_3 to form two O_2 molecules [*Sander et al.*, 2002]. Nascent $O_2(^1\Delta_g)$ is very slowly quenched by all of the species present, the fastest reaction occurring with residual O_3 to form $2O_2 + O$, with $k_{rxn} = 3.8 \times 10^{-15}$ cm^{3}s^{-1} [*Sander et al.*, 2002]. However, this reaction produces negligible additional O atoms on the several hundred μs timescale of the $CO_2(\nu_2)$-O vibrational energy transfer kinetics.

[14] For a sufficiently large CO_2 mole fraction and/or O_3 partial pressure, IR emission in the 4.3-μm spectral region was detected by the filtered InSb detector following the photolysis laser pulse. Aside from being opposite in sign, the emission had a similar temporal dependence to that of the transient absorption. The emission increased with increasing CO_2 and O_3 mole fraction, and with increasing pulse energy. It displayed as a broad, featureless emission with a maximum at approximately 4.35 μm (2300 cm^{-1}) when dispersed by a 12.8-nm resolution, 4000-nm blaze grating monochromator. The emission was presumably due to CO_2 $\nu_3 \rightarrow \nu_3 - 1$ transitions arising from excitation into high-energy υ levels. Under the data-taking conditions no long-lived emission was observed. A second, short-lived (30–40 μs) emission transient due to UV laser scatter was accounted for by detuning the diode detection laser a few line widths off the CO_2 [01^{1}0] absorption line center, measuring the transient signal, then tuning back onto resonance and repeating the measurement. The off-resonance signal was subtracted from the on-resonance signal prior to further analysis.

2.4. Photolysis Laser Profile

[15] The photolysis laser beam spatial profile was determined by assuming the energy E to be described by the normalized Gaussian function

$$E(r) = \frac{2E_{TOT}}{\pi w^2} e^{\frac{-2r^2}{w^2}}, \tag{6}$$

where r is the off-axis radial distance and w is the $1/e^2$ beam radius, both in units of cm, E_{TOT} is the integrated beam energy in units of mJ, and $E(r)$ is the r-dependent differential beam fluence in units of mJ cm^{-2} [*Demtröder*, 1996]. The beam radius w was determined by passing the laser through an adjustable iris, and fitting the transmitted energy E_{trans} to equation (7), derived from equation (6):

$$\frac{E_{trans}}{E_{TOT}} = 1 - e^{\frac{-2a^2}{w^2}}. \tag{7}$$

In equation (7), E_{trans} is the beam energy transmitted through the iris in units of mJ, a is the aperture radius, and w is the $1/e^2$ beam radius, both in units of cm. Figure 4 shows data from three different E_{TOT} values of approximately 15, 20, and 24 mJ, least squares fit to the functional form given in equation (7). All three curves are adequately fit assuming

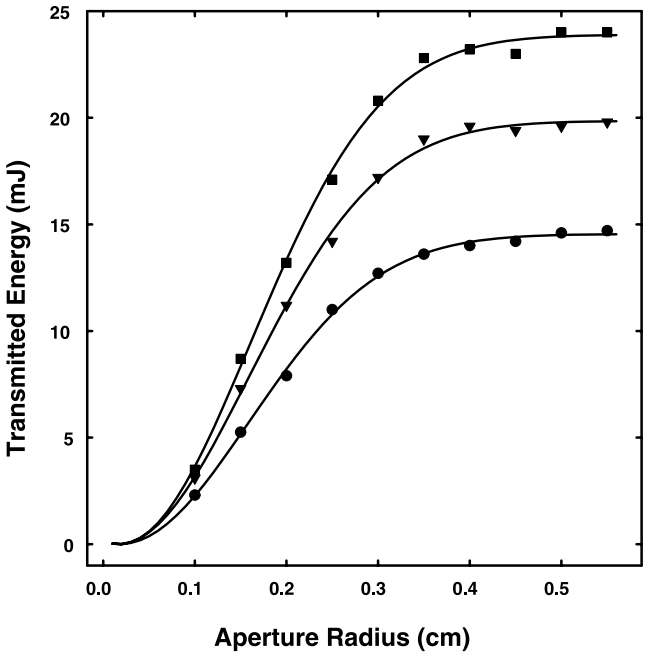

Figure 4. Transmitted photolysis laser energy as a function of adjustable iris aperture radius, for three different total energies. The data points were fit to equation (7) in the text, which predicts the dependence of the transmitted energy assuming a Gaussian spatial profile for the laser beam. The results are consistent with a $1/e^2$ beam radius of 0.284 cm.

a Gaussian line shape, the fits yielding a consistent value of $w = 0.284$ cm.

[16] The beam profile measurement can be used to specify the fractional dissociation of the O_3 as a function of photolysis beam energy and radial off-axis distance. For a given fluence $E(r)$ the fractional O_3 dissociation $F(r)$ is given by

$$F(r) = 1 - e^{\frac{-\lambda E(r)\sigma}{hc}}, \tag{8}$$

where λ is the wavelength of the photolysis laser (2.66×10^{-5} cm), σ is the absorption cross section of O_3 at the 266-nm photolysis wavelength (9.65×10^{-18} cm^2), h is Planck's constant (6.63×10^{-31} mJ s), and c is the speed of light (3.00×10^{10} cm s^{-1}). Using the measured values of E_{TOT} and w the O_3 dissociation fraction can be calculated as a function of r. Under nominal running conditions the energy $E_{TOT} = 17.0$ mJ, with 8.5 mJ entering each side of the cell following the 50/50 beam splitter. Equation (8) predicts that a fraction $F_{avg} = 0.77$ of the O_3 in the diode laser detection region was dissociated by the photolysis laser, resulting in O-atom densities ranging from 1.38×10^{13} to 2.15×10^{15} cm^{-3}. This yield is nearly independent of initial O_3 concentration. Figure 5 shows the differential beam fluence $E(r)$ and O_3 dissociation fraction $F(r)$ calculated as a function of r. Note that $F(r)$ is a less sensitive function than $E(r)$ within the diode laser detection region of $r = \pm 0.075$ cm, owing to the fact that the O_3 absorption is partially saturated.

2.5. Temperature-Jump Calculation

[17] The localized heating of the gas parcel initiated by the O_3 photolysis stimulates an expansion wave that travels radially inward from the boundary of the laser pulse, then back outward, resulting in a two-stage cooling [*Fairchild et al.*, 1982]. This process is complete on a timescale of approximately $t_{cool} = 2r/u = 7.5$ μs, where $r = 0.75$ mm and u is the speed of sound in the Xe/Ar mix, approximately 0.2 mm μs^{-1}. After this, according to *Fairchild et al.* [1982, p. 107], "the density, pressure, and temperature of the initially heated gas remain steady for a relatively long period."

[18] The initial gas temperature increase ΔT can be determined by first estimating the energy deposited in the gas mixture by the laser pulse, E_{abs}, which has units of mJ cm^{-3}. The quantity E_{abs} is equal to

$$E_{abs} = F_{avg}\left\{E_{photon} - E_{O2-O} - \left(\phi_{O2(a)} \times E_{O2(a)}\right)\right\}\rho_{O3}, \tag{9}$$

where the fractional O_3 dissociation $F_{avg} = 0.77$ as derived above, the photon energy $E_{photon} = 7.46 \times 10^{-16}$ mJ (1 eV = 1.602×10^{-16} mJ), the O_3 dissociation energy $E_{O2\text{-}O} = 1.6 \times 10^{-16}$ mJ, the $O_2(^1\Delta_g)$ photolysis quantum yield $\phi_{O2(a)} = 0.85$, the $O_2(^1\Delta_g)$ internal energy $E_{O2(a)} = 1.6 \times 10^{-16}$ mJ, and ρ_{O3} is the O_3 density in cm^{-3}. It is assumed that the $O(^1D)$, $O_2(^3\Sigma_g^-, \upsilon \geq 1)$, and $O_2(^1\Delta_g, \upsilon \geq 1)$ primary photoproducts are quenched, with their internal energy released into bath gas translation. As mentioned above, metastable $O_2(^1\Delta_g, \upsilon = 0)$ is long-lived. Nascent $O(^1D)$ is quenched quickly, but will react with any residual O_3 to produce $2O + O_2$ and $2O_2$ with a roughly 50:50 branching ratio; the former channel moderates the heating, while the latter produces more heating. The presence of minor amounts of the polyatomics CO_2, residual O_3, and O_2 introduced with the O_3 or produced through photolysis has been ignored. Since these polyatomics have higher heat capacities than Xe, they would serve to slightly moderate the temperature increase.

[19] The initial temperature increase is given by

$$\Delta T = \frac{E_{abs}}{C_v \rho_{TOT}}, \tag{10}$$

where C_v is the constant volume heat capacity of the gas mixture in mJ K^{-1} and ρ_{TOT} is the total gas density in cm^{-3}. Since the bulk of the gas mixture is Xe, the value $C_v(Xe) = 2.068 \times 10^{-20}$ mJ K^{-1} has been used. With representative experimental conditions of $[O_3] = 5 \times 10^{14}$ cm^{-3} and $\rho_{TOT} = 2.1 \times 10^{17}$ cm^{-3}, one calculates $E_{abs} = 0.17$ mJ cm^{-3} and $\Delta T = 39$ K.

[20] The final temperature T_{final} following the expansion wave is then calculated as [*Fairchild et al.*, 1982]

$$T_{final} = T_{ini}\left(\frac{T_{ini} + \Delta T}{T_{ini}}\right)^{\frac{1}{\gamma}}, \tag{11}$$

where $T_{ini} = 296$ K is the initial room temperature value, and γ is the ratio of the specific heat capacity at constant pressure to that at constant volume, taken to be the value $\gamma(Xe) = 1.67$. Equation (11) has the effect of mitigating the

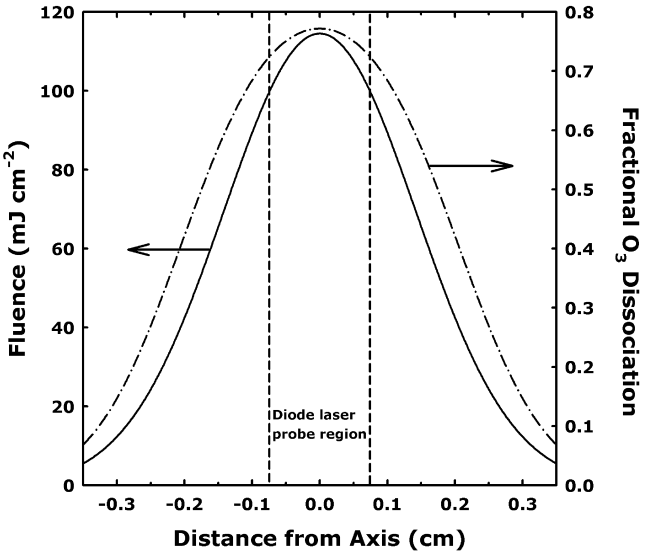

Figure 5. Photolysis laser profile, shown as a function of the radial distance off the laser centerline. Shown are profiles for the distance-dependent laser fluence and fractional O_3 dissociation. The area subtended by the diode detection laser is indicated by the two dashed lines near the center. The laser profile is plotted out to ±0.35 cm, outside of which the beam is blocked by the edge of the cell aperture. The total pulse energy prior to the beam splitter is equal to 17.0 mJ.

initial temperature jump predicted by equation (10). Using equations (10) and (11) for the gas pressures employed in this experiment, $T_{\text{final}} - T_{\text{ini}}$ typically has values in the 10–50 K range, that is, a perturbation of 3–17% relative to room temperature. The gas density decreases in inverse proportion to the fractional temperature increase $(T_{\text{final}} - T_{\text{ini}})/T_{\text{ini}}$ according to the ideal gas law. Figure 6 shows the range of O_3 densities and associated temperature jumps for the runs used in the data analysis.

[21] The value of T_{final} predicted by equation (11) can be compared to transient absorption data obtained from two or more (υ, J) transitions of the same or different υ levels, provided all of the levels are in local thermodynamic equilibrium (LTE). To obtain the absolute static and transient absorption for a given transition a three-step sequence was performed: (1) the CO_2 was pumped out and the diode laser power measured using a mechanical chopper, (2) CO_2 was reintroduced and the transmitted diode laser power measured, either by positioning the laser at line center and using the chopper or by frequency-scanning over the absorption line, and (3) the chopper was turned off, the photolysis laser turned on, and the diode laser transient size measured and added to the static absorption to obtain the transient absorption.

[22] The absorbance $A(\upsilon, J)$ is given by

$$A(\upsilon, J) = \ln\left(\frac{I_O}{I}\right), \tag{12}$$

where I_o is the diode laser signal in the absence of CO_2 and I is the laser signal with CO_2 present. For a given transition the measured absorbance was found to agree to within 5% with a prediction based on the known path length, CO_2 number density, and the literature integrated intensity S and Voigt line width γ [*Rothman et al.*, 2005]. The absorption coefficients for the various $\Delta\nu_3 = 1$, $\Delta J = \pm 1$ transitions discussed below are the same to within ±10%, [*Rothman et al.*, 2005] and the relative populations are closely approximated by the absorbance values. The reduced populations $N(\upsilon, J)$ are then written as

$$N(\upsilon, J) = \frac{A(\upsilon, J)}{(2J+1)g(\upsilon)}, \tag{13}$$

where $2J + 1$ is the rotational degeneracy and $g(\upsilon)$ is the vibrational degeneracy, equal to either 1 or 2 depending on the υ level.

[23] Under the LTE assumption the CO_2 rovibrational population distribution can be described by a single temperature via a Boltzmann plot. Figure 7 shows equations (12) and (13) applied to calculating reduced populations for several different υ, J level populations detected through diode laser absorption. The use of different υ levels allows for a relatively large x axis range and a more precise determination of the static and transient temperature. It should be noted that the relatively high O_3 density and CO_2 mole fraction used in this instance were necessary to create a large enough temperature jump to detect the higher-

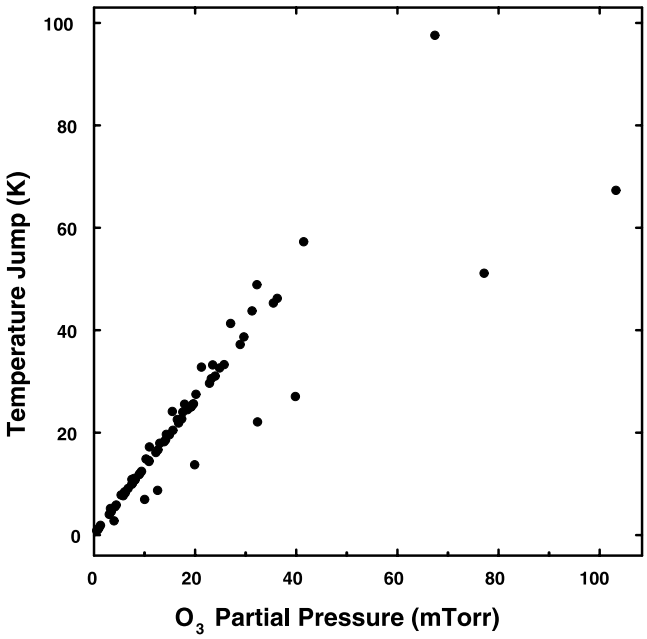

Figure 6. Calculated temperature jump versus O_3 partial pressure for the CO_2 absorption transients analyzed to obtain $k_O(\nu_2)$. The O-atom densities were estimated using O_3 absorption measurements, equation (8) to predict the 266-nm photolysis efficiency, and equations (9)–(11) to estimate the temperature jump. As can be seen, the majority of the transients had temperature jumps $\leq$50 K, representing a $\leq$17% increase in temperature from 296 K. The majority of the data points were obtained at p_{TOT} = 6.5 torr, while data from one day (defining the lower set of points) were obtained at p_{TOT} = 12.6 torr.

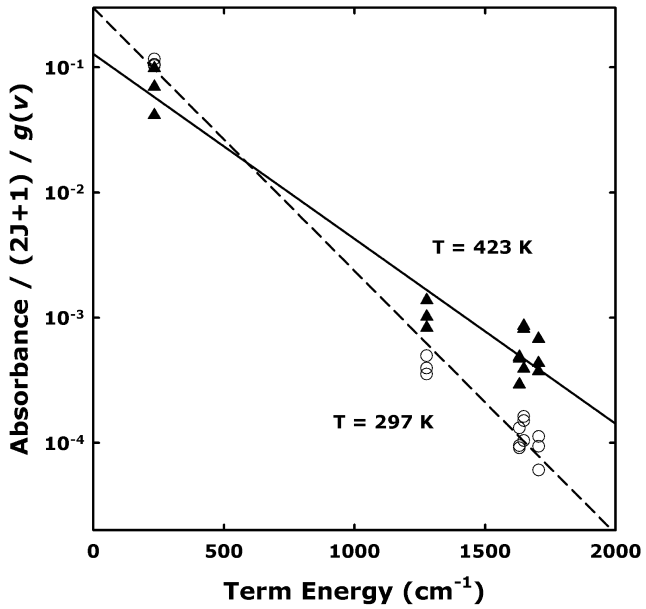

Figure 7. Relative populations for selected J states within the five lowest CO_2 vibrational levels – (00^00), (01^10), (02^20), (02^00), and (10^00), obtained from TDLAS absorbance measurements. The populations have been normalized by the appropriate rotational and vibrational state degeneracy. The open circles were obtained from the absorption of static gas mixture, and the solid triangles were obtained by adding the transient absorption to the static absorption. Note that upon laser-induced heating, all of the excited levels gain population at the expense of the ground state. The derived 125 K temperature increase is in accord with the prediction of equations (10) and (11). Conditions were as follows: laser energy E_{TOT} = 19.5 mJ, $[O_3] = 2.2 \times 10^{15}$ cm^{-3}, p_{TOT} = 5 torr containing 2.7% CO_2, 37% Ar, and 60% Xe.

energy level populations. In particular, the [00^01] population was undetectable under these conditions, while the [01^11] population could only be detected through its transient. No higher-energy populations could be detected. For the smaller O_3 and CO_2 mole fractions used in the kinetic data-taking no CO_2 populations above [01^10] could be detected.

[24] Transient absorption data utilizing several J-state transitions were obtained for the [01^10]-[01^11] band, including the $P(26)$, $P(27)$, $P(33)$, $P(39)$, and $P(47)$ lines. These were conveniently located and free of contamination from an adjacent transition. However, a competing effect that complicates the analysis is the J-dependent population redistribution stimulated by the temperature jump. This redistribution effectively offsets the signal at $t = 0$, when the photolysis laser fires, with the offset positive or negative depending on the J level. The rotational population in level J is a function of temperature according to

$$Pop_J(T) \propto e^{\frac{-(E_J-E_1)}{kT}}/T, \tag{14}$$

where the T in the denominator accounts for the temperature dependence of the rotational partition function. For two different temperatures, the population ratio in a given J state is given by

$$\frac{Pop_J(T_2)}{Pop_J(T_1)} = \frac{e^{\frac{-(E_J-E_1)}{kT_2}}}{T_2} \Big/ \frac{e^{\frac{-(E_J-E_1)}{kT_1}}}{T_1} = \frac{T_1}{T_2} e^{\frac{(E_J-E_1)}{kT_1T_2}(T_2-T_1)}. \tag{15}$$

For a given J-state population, the change in volumetric density is modified by the thermal expansion since the overall gas density decreases as T_1/T_2. The combination of the two effects is described by

$$\frac{Pop_J(T_2)}{Pop_J(T_1)} = \left(\frac{T_1}{T_2}\right)^2 e^{\frac{(E_J-E_1)}{kT_1T_2}(T_1-T_2)}. \tag{16}$$

For a small range of J values the population redistribution and density rarefaction effects nearly cancel. Figure 8 shows the relative population change for the five monitored J levels plotted against the temperature jump in K. The J = 33 population change is $\leq$1% for temperatures jumps <60 K, while the other populations are altered by 10–40%. Indeed, clear evidence is seen in the $P(47)$ data for a large positive $t = 0$ signal offset. To simplify the analysis the $P(33)$ data have been used to derive the rate constant $k_O(\nu_2)$.

[25] Short-lived absorption transients were observed superimposed on the longer timescale kinetic transients, particularly for higher O_3 mole fractions or lower bath gas pressures. Various observations showed the short-lived transients to be consistent with periodic compression and

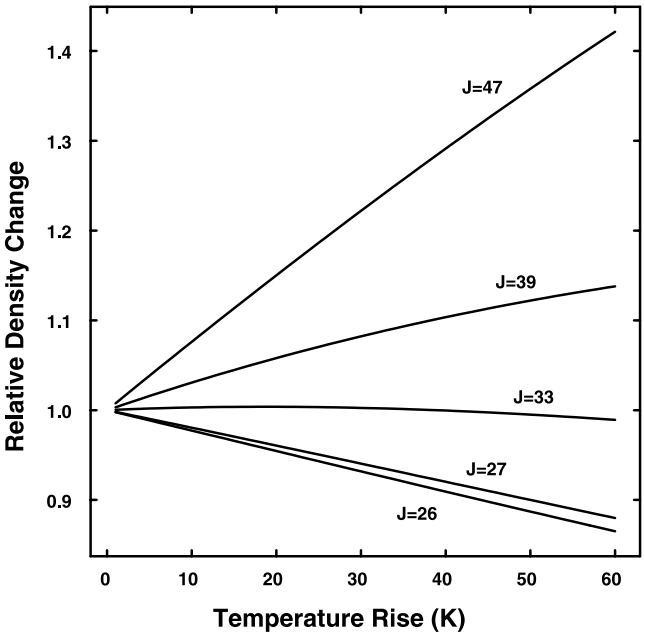

Figure 8. Predicted short-time change in volumetric density as a function of the temperature increase induced by the photolysis laser, as calculated using equation (16) for several J levels. The change results from a combination of rotational population redistribution and density rarefaction, as discussed in the text. The J = 33 level used to determine the rate coefficient $k_O(\nu_2)$ is seen to undergo little change in concentration over the predominantly $\Delta T \leq 50$ K temperature jumps used in the study.

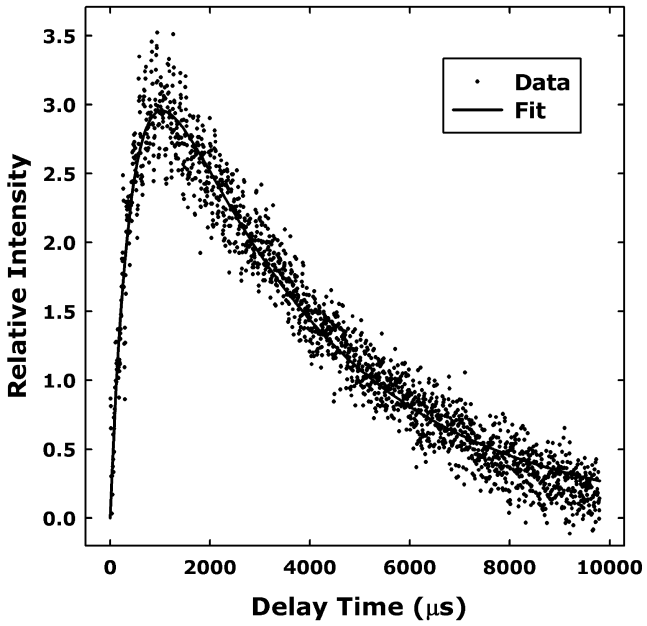

Figure 9. Sample CO_2 (01^10)-(01^11) transient absorption signal together with a fit to a double-exponential function as given in equation (17). In the global fit the rise decay constant is equal to $k_{r1}[O] + R$. The fall decay constant was observed to be constant for a given day's data and spanned the 150–350 s^{-1} range over the nine days of data. The fall decay constant characterizes population reequilibration as the gas mixture returns to the original temperature.

rarefaction induced by a recurrent sound wave. The sound wave was generated by the laser-induced heating, alternately reflecting off the cylindrical cell walls and passing through the detection region. Given the pressure-independent speed of sound $w = (RT\gamma/m)^{1/2}$, where the mass m is taken to be equal to the weighted mean of the Ar and Xe bath gas constituents, a recurrence time on the order of 100–200 μs is predicted. For two cells with radii of 20 mm and 12.7 mm and similar gas mixes, periods of 155 us and 80 us were observed in rough accord with expectation. For the 20-mm cell, the Xe mole fraction in an Ar/Xe bath gas mix was varied between 0.36–0.81, with the observed 155–195 μs period approximately proportional to $1/m^{1/2}$ again as expected. For a given gas mix, no dependence of the period on the pressure was observed. The pressure wave-induced transients were mitigated by moving the excitation/detection volume a few mm off the cell radial axis and by using relatively low O_3 mole fractions.

3. Analysis and Results

[26] An example of a transient absorption curve obtained in this work is shown in Figure 9. The smooth line in the figure was generated by fitting the data to the dual exponential function

$$I(t) = \frac{C}{(k_f - k_s)}\left(e^{-k_s t} - e^{-k_f t}\right). \quad (17)$$

As discussed by *Pollock et al.* [1993], in equation (17) the decay constant k_f describes the relatively fast evolution of the CO_2 $[01^10]$ population to its equilibrium value at the perturbed temperature, and k_s describes the slower reequilibration of the transient population as the gas mixture returns to the original temperature.

[27] To determine the best fit rate constant a large amount of data were obtained on nine different days of data-taking, with the pressure varying from 5.6–12.6 torr and the CO_2 mole fraction varying from 0.00145 to 0.00386. The data were fit simultaneously using a home-written Fortran computer program employing the Levenberg-Marquardt nonlinear least squares fitting algorithm. Two "global" parameters were found to be necessary to reproduce the data, the rate coefficient k_{r1} (equation (4)), and an "intercept" value R, which describes the O-atom density-independent contribution to the rise decay rate. In addition, a large number of "local" parameters were used, describing the day-dependent reequilibration rates and the run-dependent scaling factors. In all, a total of 355,000 data points were analyzed to determine best fit parameters. Best fit global parameter values of $k_{r1} = 2.2 \times 10^{-12}$ cm^3s^{-1} and $R = 2360$ s^{-1} were obtained with outputted error bars on the order of 1%. When the nine days of data were fit separately, similar values of k_{r1} and R were determined with mean standard deviations of approximately 10%, a more realistic value. The parameters did not change significantly when fitting subsets of the data over several different O_3 density bins. The temperature at which the measurement was performed is taken to be 318 K, equal to the gas temperature following laser excitation averaged over the experimental runs (see Figure 6). Figures 10 and 11 show the transient absorption data and nonlinear least squares best fit model curves for three different kinetic runs with different O-atom densities from a given day.

[28] In analyzing preliminary data sets it was observed that the best fit R value increased rapidly with increasing CO_2 mole fraction, and it was feared that the large values of R reflected $O(^1D)$ quenching by CO_2 followed by rapid vibrational cascade populating the ν_2 level. On the basis of the gas partial pressures and the known values for quenching of $CO_2(\nu_2)$ by the principal constituents Xe (1×10^{-16} cm^3s^{-1}) [*Allen et al.*, 1980], Ar (7×10^{-16} cm^3s^{-1}), CO_2 (5.5×10^{-15} cm^3s^{-1}), and O_2 (5.2×10^{-15} cm^3s^{-1}) [*Lunt et al.*, 1985; *Siddles et al.*, 1994], the contribution from O_3 density-independent relaxation to the R value is expected to be less than 100 s^{-1}, much lower than derived from the kinetic fit. It should be noted that the best fit value of R given above is 27 times lower than the preliminary value, while k_{r1} is the same within error, suggesting that the slope is not highly dependent on the $[CO_2]$-sensitive intercept.

[29] To better quantify the relative contributions made by temperature-jump-induced repopulation and vibrational cascade to the CO_2 $[01^10]$ transient absorption signal, a control experiment was performed utilizing various Ar and Xe bath gas mixtures. Table 1 shows the signal magnitude as a function of gas mix. The CO_2 transient signal is very large at relatively low pressure with a large CO_2 mole fraction and balance Ar. Ar is 250 times less efficient than Xe at quenching nascent $O(^1D)$, with $k_Q(Ar) = 3 \times 10^{-13}$ cm^3s^{-1} [*Schofield*, 1978]. In this case the $O(^1D)$ photolysis product is likely to excite a large fraction of the CO_2 to high

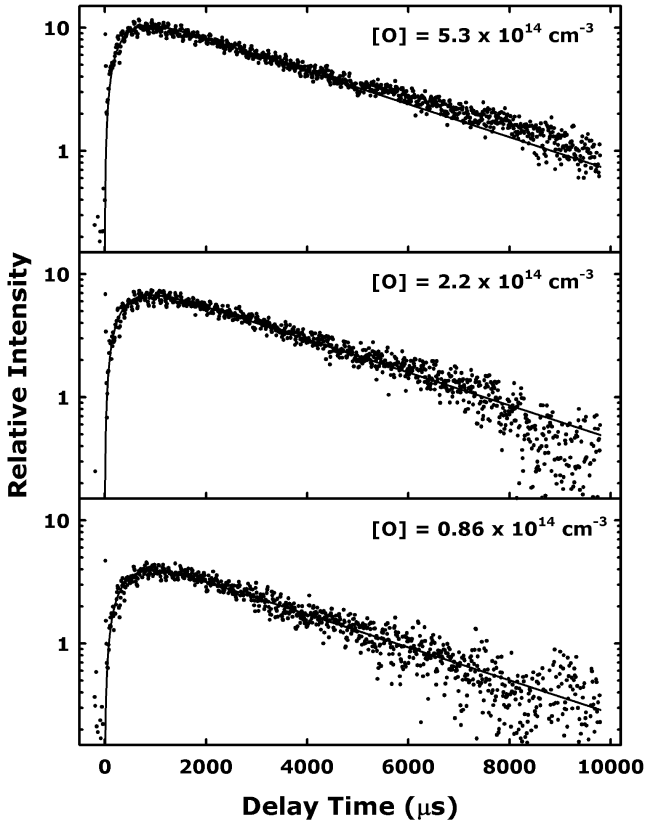

Figure 10. CO_2 (01^10)-(01^11) $P(33)$ transient absorption signal obtained on a single day for three different O-atom concentrations, plotted on a semi-log scale. Only every tenth data point is shown for clarity. The lines are the predicted population time evolution from a global fit to that day's data set. For a given transient the rise decay constant is equal to $k_{r1}[O] + R$, while the best fit fall decay constant for this day is equal to 308 s^{-1}. Overall, the O-atom density spans a factor of >50 over the nine days of data.

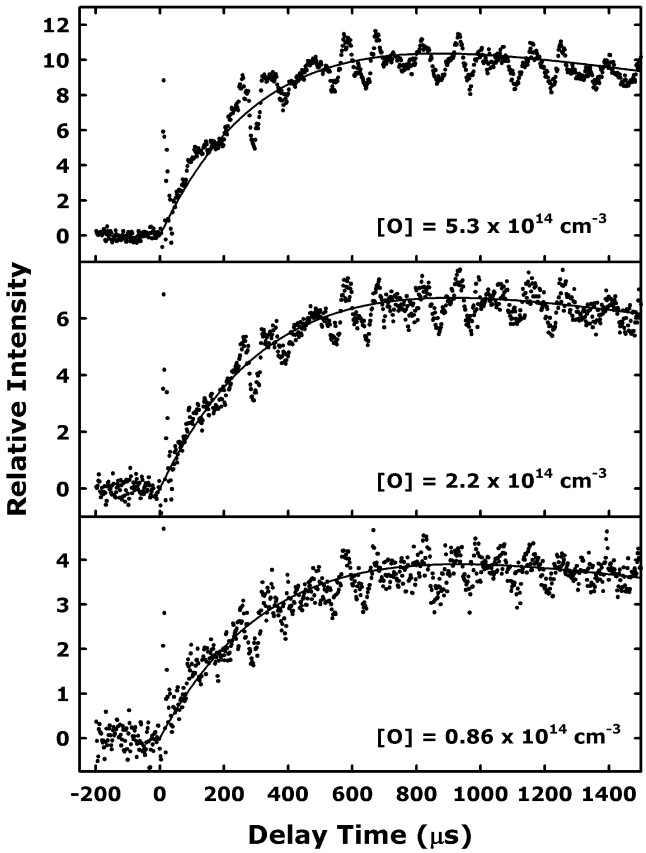

Figure 11. CO_2 (01^10)-(01^11) $P(33)$ transient absorption signal for the initial portion of the curves shown in Figure 10, plotted on a linear scale. Only every other data point is shown for clarity. The lines are the predicted population time evolution from a global fit to that day's data set. The approximately 80-μs period modulation results from residual sound wave activity as discussed in the text. For a given transient the rise decay constant is equal to $k_{r1}[O] + R$, while the best fit fall decay constant for this day is equal to 308 s^{-1}.

vibrational levels, promoting cascade. Upon raising the Ar bath gas pressure and lowering the CO_2 mole fraction the transient size decreases by a factor of three, and then by another factor of two when replacing half the Ar with Xe. Finally, on replacing the roughly 50:50 Ar/Xe mix with 94% Xe the transient size decreases by only 14%, indicating that vibrational cascade is nearly eliminated. It should be noted that the CO_2 mole fraction is about five times lower in the data used to derive k_{r1}, further discouraging the cascade effect. For these data no emission was observed in the 3.8–4.8-μm band pass, and no absorption transient could be detected for any of the higher vibrational level populations probed, including the $[02^00]$, $[02^20]$, $[10^00]$, $[03^10]$, $[00^01]$, and $[01^11]$ levels (see Figure 2).

[30] The best fit intercept R, however, low by some measures, remains a concern. As discussed above, R is 20–30 times larger than predicted on the basis of the assumption that all of the CO_2 $[01^10]$ population is being formed through collision-induced up-pumping of the $[00^00]$ population by Xe, Ar, CO_2, and O_2. The data are well fit using a model that employs a single rate coefficient k_{r1} and intercept R, while an alternative model that incorporates two independent exponentially decaying feed terms does not reproduce the data. The assembled evidence suggests that another species besides those considered is exciting ground-state CO_2 to form $CO_2(\nu_2)$.

[31] A likely scenario is that excitation of $CO_2(\nu_2)$ is being catalyzed by residual, undissociated O_3, for which the ν_2 bending mode at 701 cm^{-1} is nearly equienergetic with the CO_2 ν_2 mode. Like CO_2, any O_3 remaining in the laser-excited region will also undergo vibrational reequilibration

Table 1. Observed CO_2 $[01^10]$ $J = 33$ Transient Size Under Varying Bath Gas Mole Fractions[a]

$\chi(CO_2)$	χ(Ar)	χ(Xe)	p_{TOT}, torr	Transient Size, mV
0.25	0.75	0.0	3	20
0.016	0.984	0.0	16.5	7
0.016	0.438	0.546	16.5	3.5
0.016	0.047	0.937	16.5	3

[a]In all cases a trace amount (approximately 40 mT) of O_3 was present in addition to the gases listed.

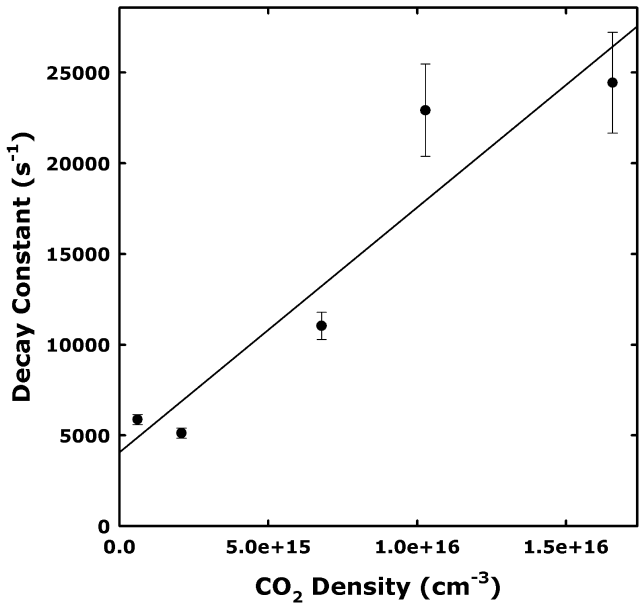

Figure 12. Best fit decay constant for CO_2 (01^10) formation as a function of CO_2 number density. The unweighted least squares fit shown gives rise to a slope and intercept of 1.35×10^{-12} cm^3s^{-1} and 4100 s^{-1}, respectively, similar to the values obtained when the global least squares fit is applied. Conditions were as follows: $[O_3] = 9.5 \times 10^{14}$ cm^{-3}, $p_{TOT} = 6$ torr containing variable CO_2 in a 18% Ar/82% Xe bath gas mixture.

at the increased gas temperature. Rate coefficients for the relevant O_3 (010) collisional quenching process

$$M + O_3(010) \xrightarrow{k_{18}} M + O_3(000) \tag{18}$$

have been measured for M = Xe (3.7×10^{-15} cm^3s^{-1}), Ar (5.8×10^{-15} cm^3s^{-1}), O_2 (2.3×10^{-14} cm^3s^{-1}) [*Zeninari et al.*, 2000] and O (3×10^{-12} cm^3s^{-1}) [*West et al.*, 1976]. On the basis of these values, formation of O_3 (010) is expected to have a fixed background rate of about 800 s^{-1} plus an additional amount depending on the O-atom concentration.

[32] Formation of O_3 (010) would be accompanied by efficient resonant vibrational energy transfer with CO_2:

$$O_3(010) + CO_2\left(00^00\right) \underset{k_{-19}}{\overset{k_{19}}{\rightleftharpoons}} O_3(000) + CO_2\left(01^10\right), \tag{19}$$

where $\Delta E = -34$ cm^{-1}. Taking the species concentrations in equation (19) to be approximated by those of the ground vibrational levels the equilibration rate R_{19} is given by [*Bernasconi*, 1976]

$$R_{19} = k_{19}[CO_2] + k_{-19}[O_3]. \tag{20}$$

Equation (20) shows that even in the limit of very small $[CO_2]$ or $[O_3]$ that the equilibration can still be rapid owing to the presence of the other constituent.

[33] Figure 12 plots the dependence of the decay constant for $CO_2(\nu_2)$ production on the CO_2 number density at constant pressure. Varying the CO_2 density over the range shown in Figure 12 had no effect on the decay constant for the longer-term thermal equilibration, as expected. The kinetic data were analyzed using the same global fit model described above to determine k_{r1}. Assuming the mechanism in equation (19), the fit yields $k_{19} = (1.4 \pm 0.3) \times 10^{-12}$ cm^3s^{-1} and $k_{-19} = (0.6 \pm 0.1) \times 10^{-12}$ cm^3s^{-1}, the latter by microscopic reversibility. For $[CO_2] = 7.6 \times 10^{14}$ cm^{-3} corresponding to $\chi_{CO2} = 0.00386$ used in the majority of the experimental runs, the decay constant for $CO_2(\nu_2)$ formation in the limit of small $[O_3]$ is predicted to be $k_{19}[CO_2] = 1100$ s^{-1}, in factor-of-two agreement with the best fit intercept value R. The decay constant also has a component proportional to $[O_3]_{residual}$ through the $k_{-19}[O_3]$ term. The process described in equation (19) contributes $0.3 \times (0.6 \times 10^{-12}) = 0.2 \times 10^{-12}$ cm^3s^{-1} to the slope used to determine k_{r1}, where the 0.3 factor takes into account the $[O_3]_{residual}/[O]$ ratio derived from the 0.77 photolysis yield. The k_{r1} value is thus revised downward to 2.0×10^{-12} cm^3s^{-1}. The 3100 ± 1000 s^{-1} best fit intercept for the Figure 12 data is roughly consistent with the predicted value of k_{-19} $[O_3]_{residual} + k_{r1}$ $[O] = 1600$ s^{-1}, where $[O_3]_{residual} = 2.2 \times 10^{14}$ cm^{-3} is taken from the known O_3 concentration and photolysis yield. Allowing for uncertainty in experimental parameters such as gas mixing and O_3 photolysis fraction, error bars of ±15% have been assigned to both the original determination of $k_O(\nu_2)$ and its correction due to $O_3(\nu_2)$ energy transfer, resulting in a final value of $k_O(\nu_2) = (1.8 \pm 0.3) \times 10^{-12}$ cm^3s^{-1}.

[34] In principle, it should be possible to gauge the influence of residual O_3 on the derived $k_O(\nu_2)$ value by varying the O_3 photolysis yield. However, it is necessary to vary the laser pulse energy substantially to create a measurable effect due to partial saturation by the photolysis laser. In a preliminary experiment, the pulse energy was varied ±25%, creating a ±10% variation in the O_3 photolysis yield. No significant trend in the derived $k_O(\nu_2)$ values over the four different photolysis yields was apparent. More extensive trials varying the photolysis yield are planned, including 100% bleaching if possible, to mitigate the effect of residual O_3 catalyzing the formation of $CO_2(\nu_2)$.

[35] While it is conceivable that some other prompt O_3 photoproduct is exciting the $CO_2(\nu_2)$ population with a rate proportional to the initial O_3 concentration, further biasing the $k_O(\nu_2)$ value upward, the other photoproducts are either present in too low concentration or are quenched too slowly to make a difference. The photoproducts include $O(^1D)$ and $O_2(^1\Delta_g)$ as well as vibrationally excited $O_2(a, \upsilon \leq 3)$ and $O_2(X, \upsilon \leq 20)$. These are considered in order:

[36] 1. For $O(^1D)$, direct excitation of CO_2 has been ruled out as discussed above. Excited O_2 could be formed through the reaction $O(^1D) + O_3$ which forms a mix of $O(^3P)$ and O_2 with an overall rate coefficient of 2×10^{-10} cm^3s^{-1}[*Sander et al.*, 2002]. However, Xe will quench >99.7% of the $O(^1D)$ for the 90% of the data with $[O_3] < 30$ mTorr. This puts an upper limit of 2×10^{12} cm^{-3} on the excited O_2 formed from the $O(^1D) + O_3$ reaction, an amount too small to significantly affect the $CO_2(\nu_2)$ population.

[37] 2. For $O_2(^1\Delta_g)$, quenching by residual O_3 could produce excited O_2, but the rate would only be about 5 s^{-1}, too slow to affect $CO_2(\nu_2)$ formation.

[38] 3. For $O_2(a, v)$ and $O_2(X, v)$, 266-nm O_3 photolysis forms $O_2(a, v = 1–3)$ in large yield [*Dylewski et al.*, 2001],

Table 2. Laboratory Determinations of the CO_2 [01^10]-O Vibrational Relaxation Rate Coefficient $K_o(\nu_2)$ at or Near Room Temperature

$k_O(\nu_2)$ ($\times 10^{-12}$ cm^3 s^{-1})	Temperature, K	Reference
1.8 ± 0.3	318	this work
1.4 ± 0.2	300–358	*Khvorostovskaya et al.* [2002]
1.2 ± 0.2	295	*Pollock et al.* [1993], *Scott et al.* [1993]
1.5 ± 0.5	300	*Shved et al.* [1991]

while the slightly shorter wavelength 248-nm O_3 photolysis produces $O_2(X, v \leq 22)$ with a broad maximum in the v = 5–10 range [*Park and Slanger*, 1994]. Rate coefficients for the quenching of $O_2(a, v = 1, 2)$ by CO_2 are in the low-to-mid 10^{-14} range (E. S. Hwang et al., Collisional removal of $O_2(a, v = 1, 2)$ by O_2, N_2, and CO_2, manuscript in preparation, 2006), too small for the process to significantly populate $CO_2(\nu_2)$. Rate coefficients for the quenching of $O_2(X, v = 8–11)$ by CO_2 are in the low-10^{-13} cm^{3}s^{-1} range [*Klatt et al.*, 1996], while for $O_2(X, v = 18)$ the CO_2-induced relaxation rate coefficient peaks at 3.8×10^{-12} cm^{3}s^{-1} [*Mack et al.*, 1996]. In the latter case, $\Delta\nu_1 = +1$ excitation in CO_2 is nearly resonant with the O_2 $v = 18 \rightarrow 17$ transition. However, for 248-nm photolysis $O_2(v = 18)$ and nearby levels are formed in only about 1% yield, translating to about 10^{12} cm^{-3}, too small to significantly affect the $CO_2(\nu_2)$ population. For 266-nm photolysis the high-v yield is expected to be even smaller.

4. Discussion

4.1. Previous Studies

[39] Relatively few laboratory studies of the O-CO_2 V-T energy transfer process have been performed. Table 2 lists the published laboratory measurements for $k_O(\nu_2)$ along with the present measurement. As can be seen, the values are in good agreement. Shved and coworkers [*Khvorostovskaya et al.*, 2002; *Shved et al.*, 1991] have performed two independent measurements of $k_O(\nu_2)$. The experiments utilized a hollow-cathode glow discharge in pure CO_2, with a total pressure on the order of 1 torr. The O-atom density, about 1% of the total, was determined from kinetic modeling of the principal production and loss mechanisms and the excited CO_2 [01^10] population detected in emission. In their initial work [*Shved et al.*, 1991] the authors performed a steady state analysis of CO_2 vibrational level populations at room temperature. In their more recent study [*Khvorostovskaya et al.*, 2002] the discharge was extinguished at regular intervals and the time evolution of the CO_2 [01^10] population observed under quasi–steady state conditions. The authors employed a large number of kinetic model assumptions in their analysis, a possible source of error.

[40] Phillips and coworkers [*Pollock et al.*, 1993; *Scott et al.*, 1993] analyzed the approach to equilibrium of the CO_2 [01^10] population following ultraviolet flash photolysis of Ar-O_3-CO_2 mixtures, using the temperature-jump method. The O_3 photolysis produced O atoms and also served to heat the mixture by approximately 12 K, giving rise to a slightly enhanced steady state CO_2 [01^10] population. The [01^10] population was detected using the same transient diode laser absorption technique employed in the present study. Unfortunately, the authors did not monitor other manifold populations to quantify the possible effects of vibrational cascading.

[41] A flow tube approach has been documented in two technical reports. *Lilenfeld* [1994] used a microwave discharge to overpopulate CO_2 [01^10], which was relaxed by O atoms produced by an O_2 microwave discharge. Slow heating of the flow tube walls by the CO_2 discharge altered the equilibrium CO_2 [01^10] concentration and was a potential source of systematic error. *Nelson et al.* [1997] encountered similar problems in their attempt to measure the rate coefficient $k_O(\nu_2)$ in a fast flow tube that employed an oven to preheat the CO_2 and overpopulate the CO_2 [01^10] level. The temperature-jump method used by Phillips and coworkers has the strong advantage of removing wall effects from the kinetic mechanism that proved so troublesome for the flow tube experiments.

[42] In recent work, *de Lara-Castells et al.* [2006] have performed fully quantum ab initio calculations of the quenching of $CO_2(\nu_2)$ by the three spin-orbit states of $O(^3P_J)$, namely J = 2,1,0. Those calculations show that for temperatures less than about 2000 K that the J = 2 sublevel dominates the quenching. This result does not present a problem for the current measurement or its interpretation. The measured $k_O(\nu_2)$ value is simply the sum of the rate coefficients for each O-atom J level. It is necessary to consider, however, the $O(^3P)$ nascent J-population distribution following quenching of $O(^1D)$ by Xe and the subsequent Xe collision-induced intersystem crossing efficiency. *Matsumi et al.* [1994] measured a nearly statistical distribution of $O(^3P)$ J populations following $O(^1D)$ quenching by Xe, with relative populations equal to 0.54:0.31:0.15 for J = 2,1,0. The populations were found to be thermalized in Xe bath gas after approximately 10 collisions, a time corresponding to a negligible 0.5 μs for the 6-torr pressure used in the present study. Thus the $O(^3P)$ J-population distribution in this work can be taken as the Boltzmann 296-K distribution of 0.74:0.21:0.05 for J = 2,1,0. Since O atoms are long-lived in the upper atmosphere they are almost certainly thermalized in that environment as well. Note that this result implies the presence of a weak temperature dependence due to the varying Boltzmann distribution of the three spin sublevels.

4.2. CO_2 Vibrational Manifold and Dynamics

[43] Known aspects of CO_2 vibrational self-relaxation have been summarized by *Levine and Bernstein* [1987]. Briefly, the symmetric stretch manifold ($m0^00$) is strongly coupled to the bend manifold ($0n^10$) via Fermi resonance interactions [*Taylor and Bitterman*, 1969]. Both the bend and asymmetric stretch manifolds are efficiently collisionally relaxed to the first excited levels [01^10] and [00^01] via near-resonant collisions with ground-state CO_2 [*Kreutz et al.*, 1987; *Lepoutre et al.*, 1977; *Orr and Smith*, 1987; *Siddles et al.*, 1994]. Thus the excited levels that are presumably longer-lived following collisional excitation reduce to [01^10], [00^01], and [01^11]. The first of these is the level under study in this work. The latter two populations with ν_3 asymmetric stretch excitation are probably the chief concern regarding delayed feed of [01^10]. Note that the [01^10] population is only slowly quenched by CO_2 and most other species, since it involves V-T energy transfer.

[44] Several low-lying CO_2 vibrational level populations resulting from $O(^1D)$-CO_2 single collisions were monitored by *Zhu et al.* [1990]. They observed modest translational and rotational excitation, consistent with inelastic scattering between CO_2 and translationally excited $O(^1D)$ but not electronic quenching. Their calculations imply that the $O(^1D)$-CO_2 E-V energy transfer process should result in CO_2* containing a very high level of rotational and translational excitation, inconsistent with their observations. For the pressures used in our experiments, the energy deposited in the R,T degrees of freedom would likely be quenched rapidly and are not a major concern. If higher vibrational levels are significantly populated, the downward cascade from them into the $[01^10]$ level could complicate the interpretation of the kinetic observations. However, it is not obvious that this has been a major problem in previous experiments. For instance, *Pollock et al.* [1993] point out that such cascading would produce an obvious perturbation on the double-exponential relaxation behavior described by equation (17). They observed reproducible but only very slight nonexponential effects on the shape of the decay curve. *Lilenfeld* [1994] checked more directly for the presence of higher-lying vibrational populations, using a diode laser to probe populations in six different vibrational levels. At a point well downstream of his microwave discharge source, only the $[01^10]$ level was significantly populated.

[45] Nonexponential behavior in the $[01^10]$ transient curve was observed in the initial stages of this study when larger CO_2 and O_3 mole fractions were used. These conditions helped promote an undesirably large temperature jump and increased direct excitation of CO_2 by $O(^1D)$ [*Sedlacek et al.*, 1989; *Zhu et al.*, 1990]. In later experiments the CO_2 and O_3 mole fractions were lowered to minimize the higher-υ-level populations, making use of TDLAS monitoring of various CO_2 (mn^lp) level populations. In particular, it was found that using a large excess of Xe bath gas greatly reduced the nascent CO_2 higher-υ-level populations, for example, the $[00^01]$ asymmetric stretch population. For example, with 3.1% CO_2 in Xe at 5 torr, the $[00^01]$ population absorption transient was observed to be 10 times smaller in magnitude than the $[01^10]$ transient. When the CO_2 was lowered to 1.2%, the $[00^01]$ transient was 400 times smaller than the $[01^10]$ transient. Under the typical conditions of <0.5% CO_2 in Xe at >5 torr total pressure, the $[00^01]$ transient was unobservable and it was concluded that cascade from higher vibrational states was negligibly small.

4.3. Field Measurements

[46] CO_2-O vibration-to-translation (V-T) energy transfer has been shown to be important through the analysis of aeronomical data. *Sharma and Wintersteiner* [1990] through analysis of CO_2 emission from the terrestrial MLT region, have determined that the CO_2-O V-T transfer rate must be high to explain the observed radiance levels. They derived a value of $k_O(\nu_2) = (6 \pm 3) \times 10^{-12}$ cm^{3}s^{-1} for a temperature of 300 K. *Rodgers et al.* [1992] using earthlimb CO_2 absorption data, showed that the populations giving rise to the 15-μm fundamental and first hot bands of the CO_2 primary isotope were in LTE to about 95–100 km. Similar to the Sharma and Wintersteiner result, their observations implied efficient O-CO_2 V-T coupling. Assuming a high V-T efficiency also reduced some of the problems associated with understanding the heat budget of the Venusian thermosphere [*Keating and Bougher*, 1992]. *Lopez-Puertas et al.* [1992] derived $k_O(\nu_2) = (3-6) \times 10^{-12}$ cm^{3}s^{-1} on the basis of an analysis of CO_2 radiance from ATMOS spectra, and have used $k_O(\nu_2) = 3 \times 10^{-12}$ cm^{3}s^{-1} in predictive non-LTE models [*Lopez-Puertas et al.*, 1998; *Lopez-Valverde and Lopez-Puertas*, 1994]. *Bougher et al.* [1994] report that data from Venus and Mars constrain the value of $k_O(\nu_2)$ to $2-4 \times 10^{-12}$ cm^{3}s^{-1} for 300 K. *Vollmann and Grossmann* [1997], on the other hand, report that their analysis of 15-μm emission observed in four SISSI (Spectroscopic Infrared Structure Signatures Investigation) sounding rocket launches confirms the 300-K value of $k_O(\nu_2) = 1.5 \times 10^{-12}$ cm^{3}s^{-1} measured by *Shved et al.* [1991].

[47] Recent publications [*Bougher et al.*, 1994; *Lopez-Puertas and Lopez-Valverde*, 1995; *Sharma and Roble*, 2002] have repeatedly stressed the need for an accurate measurement of $k_O(\nu_2)$ in order to refine computations of the thermal balance in the terrestrial MLT region. Given the agreement among the room temperature laboratory results in Table 2, the logical next steps are to resolve the discrepancy between the laboratory and aeronomically derived $k_O(\nu_2)$ values and to characterize the temperature dependence in the 150–500 K range. The CO_2 concentration is variable at altitudes above 75 km [*Lopez-Puertas and Taylor*, 1989], and thus the O-CO_2 radiative cooling mechanism depends on variable O and CO_2 mixing ratios and a variable temperature. Accurate knowledge of $k_O(\nu_2)$ as a function of temperature will help elucidate the strong interplay between chemistry and dynamics that is a consequence of these variabilities. It is also required for NASA's Office of Space Science Thermosphere-Ionosphere-Mesosphere Energetics and Dynamics (TIMED) mission [*Mlynczak*, 1997]. The TIMED Sounding of the Atmosphere using Broadband Emission Radiometry (SABER) experiment is measuring emission from the ν_2 bands of CO_2 at 15-μm wavelength. These measurements will be used to derive the kinetic temperature of the atmosphere and the IR cooling rates associated with CO_2 emission. The rate coefficient $k_O(\nu_2)$ is a key parameter in the SABER analyses and is necessary for the SABER experiment to achieve its accuracy goals with respect to mesospheric temperature measurements and cooling rate calculations [*Houghton*, 1970; *Mertens et al.*, 2001; *Mlynczak*, 2001].

[48] There is also mounting evidence that increasing levels of CO_2 and other greenhouse gases are causing the upper atmosphere to cool and contract, leading to a significant density decrease. Evidence for this "greenhouse cooling" effect has been documented by many researchers, analyzing a variety of data sets. In particular, recent analyses of satellite orbital trajectories are consistent with a decrease in thermospheric density over the last few decades. *Keating et al.* [2000] observed a 10% decrease in atmospheric density at an altitude of 380 km since 1976. *Emmert et al.* [2004] observed a decrease of 2% per decade at 200 km and 4% per decade at 700 km since 1966. A study by *Marcos and Grossbard* [2004] indicates a 5% decrease in density at 400 km between 1970 and 2000. Other evidence of thermospheric cooling includes observation of polar mesospheric clouds at much lower latitudes than had

previously been observed [*Olivero and Thomas*, 2001]. Somewhat more speculative evidence includes observed decreases in the altitudes of several layers of the ionosphere [*Bremer*, 2001]. Several groups have run models suggesting that, for a given altitude, the thermosphere could respond to a doubling of CO_2 by a 40 to 50 K decrease in temperature, and, perhaps more significantly, a factor of three decrease in density [*Akmaev and Fomichev*, 1998; *Roble*, 1995]. Thus, understanding the O-CO_2 vibrational energy transfer process could be key in accurately predicting long-term changes in the temperature and density structure of the upper atmosphere.

5. Conclusions

[49] The rate coefficient $k_O(\nu_2)$ for the vibrational deactivation of the bend-excited state CO_2 [01^10] by oxygen atoms has been measured. The temperature-jump method was used, in which 266-nm photolysis of variable amounts of O_3 in a trace CO_2/predominately Xe gas mix produced a high yield of O atoms and provided modest heating. The CO_2 [01^10] population evolution was monitored using time-resolved, tunable diode laser absorption spectroscopy in the 4.3-μm spectral region. The CO_2 mole fraction was kept as low as possible to minimize competing energy transfer pathways. Under the appropriate conditions no higher-energy CO_2 υ-level population transients could be detected. A global, nonlinear least squares fitting algorithm was employed to determine the rate coefficient $k_O(\nu_2) = (1.8 \pm 0.3) \times 10^{-12}$ cm^3s^{-1}, in good agreement with results from previous experiments. The value is a factor of 2–3 lower than many aeronomically derived estimates, however, a discrepancy that needs to be resolved. The $CO_2(\nu_2)$-O vibrational transfer efficiency is a crucial input for aeronomic models of the energy budget of Earth, Mars, and Venus, and for the interpretation of the SABER IR sounding measurements on NASA's TIMED satellite, currently in orbit.

[50] **Acknowledgments.** This research was supported by the NASA Office of Space Science under award W10,059, and by the Air Force Office of Scientific Research under project 2303, task 92VS04COR. ESH performed this work under contract F19628-98-C-0058 with AFRL. KJC's work on this project was supported by the Clare Boothe Luce Program of the Henry Luce Foundation and the Camille & Henry Dreyfus Foundation. The authors would like to thank Richard Copeland of SRI International for helpful discussions and Kristin Cashman of Bucknell University for her assistance with the photolysis laser profile measurements.

[51] Zuyin Pu thanks Tom Slanger and Leon Phillips for their assistance in evaluating this paper.

References

Akmaev, R. A., and V. I. Fomichev (1998), Cooling of the mesosphere and lower thermosphere due to doubling of CO_2, *Ann. Geophys.*, *16*, 1501–1512.

Allen, D. C., T. Scragg, and C. J. S. M. Simpson (1980), Low temperature fluorescence studies of the deactivation of the bend-stretch manifold of CO_2, *Chem. Phys.*, *51*, 279–298.

Bernasconi, C. F. (1976), *Relaxation Kinetics*, 288 pp., Academic, New York.

Bougher, S. W., D. M. Hunten, and R. G. Roble (1994), CO_2 cooling in terrestrial planet thermospheres, *J. Geophys. Res.*, *99*, 14,609–14,622.

Bremer, J. (2001), Trends in the thermosphere derived from global ionosonde observations, *Adv. Space Res.*, *28*, 997–1006.

Castle, K. J., E. S. Hwang, and J. A. Dodd (2003), Laboratory studies of CO2 (ν_2)-O vibrational energy transfer, *Proc. SPIE*, *5235*, 276–287.

de Lara-Castells, M. P., M. I. Hernández, G. Delgado-Barrio, P. Villarreal, and M. López-Puertas (2006), Vibrational quenching of CO_2 (010) by collisions with O (^{3}P) at thermal energies: A quantum mechanical study, *J. Chem. Phys.*, *124*, 164302.

Demtröder, W. (1996), *Laser Spectroscopy: Basic Concepts and Instrumentation*, 2nd ed., 924 pp., Springer, New York.

Dylewski, S. M., J. D. Geiser, and P. L. Houston (2001), The energy distribution, angular distribution, and alignment of the O(^{1}D$_2$) fragment from the photodissociation of ozone between 235 and 305 nm, *J. Chem. Phys.*, *115*, 7460–7473.

Emmert, J. T., J. M. Picone, J. L. Lean, and S. H. Knowles (2004), Global change in the thermosphere: Compelling evidence of a secular decrease in density, *J. Geophys. Res.*, *109*, A02301, doi:10.1029/2003JA010176.

Fairchild, P. W., G. P. Smith, and D. R. Crosley (1982), A laser pyrolysis/laser fluorescence technique for combustion chemical kinetics, paper presented at Nineteenth International Symposium on Combustion, Combustion Inst., Haifa, Israel, 8–13 Aug.

Houghton, J. T. (1970), Absorption and emission by carbon-dioxide in the mesosphere, *Q. J. R. Meteorol. Soc.*, *96*, 767–770.

Keating, G. M., and S. W. Bougher (1992), Isolation of major Venus thermospheric cooling mechanism and implications for Earth and Mars, *J. Geophys. Res.*, *97*, 4189–4197.

Keating, G. M., R. H. Tolson, and M. S. Bradford (2000), Evidence of long term global decline in the Earth's thermospheric densities apparently related to anthropogenic effects, *Geophys. Res. Lett.*, *27*, 1523–1526.

Khvorostovskaya, L. E., I. Y. Potekhin, G. M. Shved, V. P. Ogibalov, and T. V. Uzyukova (2002), Measurement of the rate constant for quenching CO_2 [01^10] by atomic oxygen at low temperatures: Reassessment of the rate of cooling by the CO_2 15–μm emission in the lower thermosphere, *Atmos. Ocean. Phys.*, *38*, 613–624.

Klatt, M., I. W. M. Smith, A. C. Symonds, R. P. Tuckett, and G. N. Ward (1996), State-specific rate constants for the relaxation of O_2 ($X^3\Sigma_g^-$, v = 8–11) in collisions with O_2, N_2, NO_2, CO_2, N_2O, CH_4, and He, *J. Chem. Soc. Faraday Trans.*, *92*, 193–199.

Kreutz, T. G., J. A. O'Neill, and G. W. Flynn (1987), Diode laser absorption probe of vibration-vibration energy transfer in CO_2, *J. Phys. Chem.*, *91*, 5540–5543.

Lepoutre, F., G. Louis, and H. Manceau (1977), Collisional relaxation in CO_2 between 180 K and 400 K measured by the spectrophone method, *Chem. Phys. Lett.*, *48*, 509–514.

Levine, R. D., and R. B. Bernstein (1987), *Molecular Reaction Dynamics and Chemical Reactivity*, second ed., 535 pp., Oxford Univ. Press, New York.

Lilenfeld, H. V. (1994), Deactivation of vibrationally-excited NO and CO_2 by O-atoms, *PL-TR-94–2180*, 24 pp., Phillips Laboratory, Hanscom Air Force Base, Mass.

Lopez-Puertas, M., and M. A. Lopez-Valverde (1995), Radiative energy balance of CO_2 non-LTE infrared emissions in the Martian atmosphere, *Icarus*, *114*, 113–129.

Lopez-Puertas, M., and F. W. Taylor (1989), Carbon dioxide, 4, 3–μm emission in the Earth's atmosphere: A comparison between Nimbus 7 SAMS measurements and non-local thermodynamic equilibrium radiative transfer calculations, *J. Geophys. Res.*, *94*, 13,045–13,068.

Lopez-Puertas, M., M. A. Lopez-Valverde, C. P. Rinsland, and M. R. Gunson (1992), Analysis of the upper atmospheric CO_2 (ν_2) vibrational temperatures retrieved from ATMOS-Spacelab 3 observations, *J. Geophys. Res.*, *97*, 20,469–20,478.

Lopez-Puertas, M., G. Zaragoza, M. A. Lopez-Valverde, and F. W. Taylor (1998), Non local thermodynamic equilibrium (LTE) atmospheric limb emission at 4. 6 μm, 1, An update of the CO_2 non-LTE radiative transfer model, *J. Geophys. Res.*, *103*, 8499–8513.

Lopez-Valverde, M. A., and M. Lopez-Puertas (1994), A non-local thermodynamic equilibrium radiative transfer model for infrared emissions in the atmosphere of Mars, 1, Theoretical basis and nighttime populations of vibrational levels, *J. Geophys. Res.*, *99*, 13,093–13,115.

Lunt, S. L., C. T. Wickham-Jones, and C. J. S. M. Simpson (1985), Rate constants for the deactivation of the 15 μm band of carbon dioxide by the collision partners CH_3F, CO_2, N_2, Ar, and Kr over the temperature range 300 to 150 K, *Chem. Phys. Lett.*, *115*, 60–64.

Mack, J. A., K. Mikulecky, and A. M. Wodtke (1996), Resonant vibration-vibration energy transfer between highly vibrationally excited O_2 ($X^3\Sigma_g^-$, v = 15–26) and CO_2, N_2O, N_2, and O_3, *J. Chem. Phys.*, *105*, 4105–4116.

Marcos, F. A., and N. J. Grossbard (2004), Long-term thermospheric trends based on satellite drag analysis, *Eos Trans. AGU*, *85*(17), *Jt. Assem. Suppl.*, Abstract SA53A-04.

Matsumi, Y., Y. Inagaki, G. P. Morley, and M. Kawasaki (1994), Fine structure branching ratios and translational energies of O (^{3}P$_j$) atoms produced from collision induced intersystem crossing of O (^{1}D) atoms, *J. Chem. Phys.*, *100*, 315–324.

Mertens, C. J., M. Mlynczak, M. Lopez-Puertas, P. P. Wintersteiner, R. H. Picard, J. R. Winick, L. L. Gordley, and J. M. Russell III (2001), Retrieval of mesospheric and lower thermospheric kinetic temperature from

measurements of CO_2 15 μm Earth limb emission under non-LTE conditions, *Geophys. Res. Lett.*, *28*, 1391–1394.

Mlynczak, M. (1997), Energetics of the mesosphere and lower thermosphere and the SABER experiment, *Adv. Space Res.*, *20*, 1177–1183.

Mlynczak, M. (2001), A contemporary assessment of the mesospheric energy budget, in *Atmospheric Science Across the Stratopause, Geophys. Monogr. Ser.*, vol. 123, edited by D. E. Siskind, S. D. Eckermann, and M. E. Summers, pp. 37–52, AGU, Washington, D. C.

Nelson, D. D., P. Villalta, M. S. Zahniser, and C. E. Kolb (1997), Laboratory kinetic studies of OH and CO_2 relevant to upper atmospheric radiation balance, *Final Rep. NASW-4848*, 8 pp., Natl. Tech. Inf. Serv., Springfield, Va.

Olivero, J. J., and G. E. Thomas (2001), Evidence for changes in greenhouse gases in the mesosphere, *Adv. Space Res.*, *28*, 931–936.

Orr, B. J., and I. W. M. Smith (1987), Collision-induced vibrational energy transfer in small polyatomic molecules, *J. Phys. Chem.*, *91*, 6106–6119.

Park, H., and T. G. Slanger (1994), O_2 (X, $v = 8–22$) 300 K quenching rate coefficients for O_2 and N_2, and $O_2(X)$ vibrational distribution from 248 nm O_3 photodissociation, *J. Chem. Phys.*, *100*, 287–300.

Pollock, D. S., G. B. I. Scott, and L. F. Phillips (1993), Rate constant for quenching of CO_2 (010) by atomic oxygen, *Geophys. Res. Lett.*, *20*, 727–729.

Roble, R. G. (1995), Major greenhouse cooling (yes, cooling): The upper atmosphere response to increased CO_2, *Rev.*, 539–546.

Rodgers, C. D., F. W. Taylor, A. H. Muggeridge, M. Lopez-Puertas, and M. A. Lopez-Valverde (1992), Local thermodynamic equilibrium of carbon dioxide in the upper atmosphere, *Geophys. Res. Lett.*, *19*, 589–592.

Rothman, L. S., et al. (2005), The HITRAN 2004 molecular spectroscopic database, *J. Quant. Spectrosc. Radiat. Transfer*, *96*, 139–204.

Sander, S. P., et al. (2002), Chemical kinetics and photochemical data for use in atmospheric studies: Evaluation number 14, *JPL Publ.*, *02–25*.

Schofield, K. (1978), Rate constants for the gaseous interactions of O(2 $^1D_2$) and O(2 $^1S_0$): A critical evaluation, *J. Photochem.*, *9*, 55–68.

Scott, G. B. I., D. S. Pollock, and L. F. Phillips (1993), Temperature-jump and trajectory studies of the quenching of CO_2 (010) by atomic oxygen, *J. Chem. Soc. Faraday Trans.*, *89*, 1183–1188.

Sedlacek, A. J., D. R. Harding, R. E. Weston Jr., T. G. Kreutz, and G. W. Flynn (1989), Probing the $O(^1D) + CO_2$ reaction with second derivative modulated diode laser spectroscopy, *J. Chem. Phys.*, *91*, 7550–7556.

Sharma, R. D., and R. G. Roble (2002), Cooling mechanisms of the planetary thermospheres: The key role of O atom vibrational excitation of CO_2 and NO, *Chem. Phys. Phys. Chem.*, *3*, 101–103.

Sharma, R. D., and P. P. Wintersteiner (1990), Role of carbon dioxide in cooling planetary thermospheres, *Geophys. Res. Lett.*, *17*, 2201–2204.

Shved, G. M., L. E. Khvorostovskaya, I. Y. Potekhin, A. I. Dem'yanikov, A. A. Kutepov, and V. I. Fomichev (1991), Measurement of the quenching rate constant of CO_2 [01^10]-O collisions and its significance for the thermal regime and radiation in the lower thermosphere, *Atmos. Ocean. Phys.*, *27*, 295–299.

Siddles, R. M., G. J. Wilson, and C. J. S. M. Simpson (1994), The vibrational deactivation of the [00^01] and [01^10] modes of CO_2 measured down to 140 K, *Chem. Phys.*, *189*, 779–791.

Taylor, R. L., and S. Bitterman (1969), Survey of vibrational relaxation data for processes important in the $CO_2–N_2$ laser system, *Rev. Mod. Phys.*, *41*, 26–47.

Vollmann, K., and K. U. Grossmann (1997), Excitation of 4. 3 μm CO_2 emissions by $O(^1D)$ during twilight, *Adv. Space Res.*, *20*, 1185–1189.

West, G. A., R. E. Weston Jr., and G. W. Flynn (1976), Deactivation of vibrationally excited ozone by $O(^3P)$ atoms, *Chem. Phys. Lett.*, *42*, 488–493.

Wintersteiner, P. P., R. H. Picard, R. D. Sharma, J. R. Winick, and R. A. Joseph (1992), Line-by-line radiative excitation model for the non-equilibrium atmosphere: Application to CO_2 15–μm emission, *J. Geophys. Res.*, *97*, 18,083–18,117.

Zeninari, V., B. A. Tikhomirov, Y. N. Ponomarev, and D. Courtois (2000), Photoacoustic measurements of the vibrational relaxation of the selectively excited ozone (ν_3) molecule in pure ozone and its binary mixtures with O_2, N_2, and noble gases, *J. Chem. Phys.*, *112*, 1835–1843.

Zhu, L., T. G. Kreutz, S. A. Hewitt, and G. W. Flynn (1990), Diode laser probing of vibrational, rotational, and translational excitation of CO_2 following collisions with $O(^1D)$, I, Inelastic scattering, *J. Chem. Phys.*, *93*, 3277–3288.

K. J. Castle, K. M. Kleissas, and J. M. Rhinehart, Department of Chemistry, Bucknell University, Lewisburg, PA 17837, USA.

J. A. Dodd, Air Force Research Laboratory, Space Vehicles Directorate, 29 Randolph Road, Hanscom Air Force Base, MA 01731, USA. (james.dodd@hanscom.af.mil)

E. S. Hwang, Stewart Radiance Laboratory, 139 The Great Road, Bedford, MA 01730, USA.